IEEE Access
Multidisciplinary | Rapid Review | Open Access Journal

Received 29 December 2023, accepted 28 February 2024, date of publication 7 March 2024, date of current version 26 April 2024.

Digital Object Identifier 10.1109/ACCESS.2024.3374778

RESEARCH ARTICLE

Novel Autonomous Self-Aligning Wireless Power Transfer for Improving Misalignment

MILAD BEHNAMFAR, (Graduate Student Member, IEEE), MOHD TARIQ, (Senior Member, IEEE), AND ARIF I. SARWAT, (Senior Member, IEEE)

Department of Electrical and Computer Engineering, Florida International University, Miami, FL 33174, USA

Corresponding author: Arif I. Sarwat (asarwat@fiu.edu)

This work was supported in part by the U.S. Department of Energy (DOE) under Grant DE-NA0004109.

ABSTRACT A novel autonomous self-aligning wireless power transfer system is proposed to address the issue of misalignment in the stationary wireless charging of electric vehicles. Misalignment between transmitter and receiver is the biggest obstacle in the charging process of wireless charging of electric vehicles that hampered the widescale adoption of this technology. To improve the misalignment performance, a moveable transmitter is proposed, in which the transmitter pad is mounted on a robot. The robot is equipped with a magnetic field sensor located at the center of the circular transmitter pad. Employing the proposed algorithm, the transmitter's coil mounted on the robot follows the receiver based on measuring the magnetic field. In this case, by having misalignment, the robot moves the transmitter pad to remove misalignment and create alignment. For validating the proposed self-aligning mechanism, an experiment test has been done, and the experimental results show the effectiveness of the proposed mechanism in aligning the transmitter pad with the receiver pad. The design process and implementation of the robot by considering the transmitter's coil weight and the required torque to move the transmitter's coil are detailed.

INDEX TERMS Coupling coefficient, inductive power transfer (IPT), magnetic field sensor, misalignment performance, self-aligning mechanism, robot, stationary charging, wireless power transfer.

I. INTRODUCTION

Electric vehicles have witnessed a surge in popularity in recent years as they offer a solution to the environmental problems associated with fossil fuel vehicles. Many automakers have shifted their focus towards the production of electric vehicles, leading to their widespread commercialization. However, plug-in charging of electric vehicles suffers from range anxiety and a long duration time of charging. In addition, plug-in charging methods require users to physically connect with heavy and potentially dirty chargers, which can be inconvenient. Furthermore, this approach can be hazardous in rainy or snowy weather. Wireless power transfer (WPT) is an emerging technology appreciated for its automated, safe, and convenient characteristics, making it suitable for various conditions. These advantages have led to growing interest in wireless charging for electric vehicles (EVs) in recent years [1].

In the Wireless charging systems the charging process can automatically start without human interference, when the receiver installed under the chassis of the electric vehicle is aligned with the transmitter's pad underground. Wireless power transfer based on energy transfer is classified as Inductive power transfer (IPT) and Capacitive power transfer (CPT), utilizing the magnetic field and electric field respectively to transfer power [2]. The CPT system offers two benefits over the IPT system. First and foremost, the CPT system is insensitive to nearby metal objects, and secondly, due to using metal plates to transfer power, the CPT system is cost-efficient. However, the CPT system efficiency is much lower than the IPT system, and it has safety issues due to the electric field emission to the environment around

The associate editor coordinating the review of this manuscript and approving it for publication was Eyuphan Bulut.

the coupler [3]. Because of the mentioned reasons, the IPT system is widely used for wireless charging of electric vehicles.

The wireless power transfer for charging electric vehicles is classified into two groups: stationary and dynamic charging. In the context of stationary charging, commencing the charging process simply entails parking the vehicle above the transmitter's pad, which is installed beneath the ground. Dynamic charging enables electric vehicles to be charged while driving, which increases the driving range and decreases the battery's weight and cost [4]. In both technologies, misalignment is the biggest hurdle to effectively charging electric vehicles. In dynamic charging, the misalignment gives rise to coupling variation between the receiver and transmitter's coil, which lead to power pulsation at the battery side. Power pulsation is harmful to the battery's lifetime. Misalignment for the stationary charging scenario is even worse, which in most cases, ceases the power transfer from the primary side to the secondary side.

In WPT systems, maintaining proper alignment is a significant issue depending on standards and guidelines. When the transmitting and receiving coils are not properly aligned, it can lead to problems such as increased flux leakage and reduced mutual inductance, resulting in a drop in transfer efficiency. This is especially critical in high-power systems, where even minor misalignment can lead to substantial power losses. Therefore, it is crucial to address misalignment to ensure and optimize efficiency [5]. It is difficult to align the transmitter and receiver coils perfectly in stationary charging of electric vehicles as it relies on the driver, vehicle, and the environment. The fluctuation might be vertical, lateral, rotational, or angular. Based on the SAE J2954 standard, the wireless power transfer systems for charging electric vehicles should have the characteristic of misalignment tolerance in both horizontal and vertical directions to some extent [6]. Scholars attempt to alleviate the impact of misalignment by modifying the coil and core structure and dimension. Circular and rectangular pads are widely adopted due to their simplicity and minimal required components, leading to a decrease in the usage of copper winding. However, these configurations exhibit poor performance characterized by low coupling coefficients and limited tolerance for misalignment [7]. For improving misalignment performance, DD coil structure was proposed which shows a superior performance in tolerating misalignment compared to circular and rectangular structure [8]. An extra quadrature Q coil can be introduced to the dual DD coil structure. By placing the Q coil solely on the receiver side, the misalignment tolerance of the IPT system can be enhanced. Furthermore, by installing Q coils on both the transmitter and receiver sides, the power transmitted via the IPT system can be increased, as the transmitter's Q coil can deliver power to the receiver's Q coil [9]. The Bipolar Pad, characterized as a multi-coil pad, comprises two larger D pads that overlap each other and exhibits performance equivalent to the DDQ pad, while using approximately 25% less copper [10]. The tripolar power pad (TPP) is composed of three mutually decoupled coils that generate a polarized magnetic field for transferring power, which demonstrate a better performance in dealing with misalignment [11].

Integrating the compensation inductor with the main coil, due to cross coupling arising from magnetic integration, can boost the misalignemt tolerance [12]. Besides integrating the compensation inductor into the main coil magnetically, it was demonstrated that incorporating magnetic integration of the reverse coil can also help mitigate mutual inductance variations caused by misalignment in IPT systems [13]. A magnetic integration approach for an LCC-compensated IPT system is proposed in [14], which this approach involves integrating all inductors within the LCC resonant network into the main magnetic coupler, and integrating a coil in reverse series with the transmitting coil at the transmitter side. A combined dual-coupled IPT system with a CPT system is proposed in [15], which shows a high tolerance to misalignment, maintaining at least 66.7% of well-aligned power at 200mm misalignment.

Recently, metamaterials have been introduced to improve misalignment performance. Metamaterials, being artificial constructs, possess unique features such as negative refraction due to their organized periodic structure [16]. Metamaterials, owing to their distinctive electromagnetic properties can enhance the distribution of the magnetic field around the receiver, improve the coupling between coils, and increase the efficiency of the wireless power transfer (WPT) system [17]. Authors in [18] incorporate a high dielectric constant metamaterial plate in the WPT system, which led to a significant improvement in the system efficiency. This improvement is particularly evident in the presence of lateral or angular misalignment of the transmitting and receiving coils, thanks to the strong magnetic dipole behavior produced by the high dielectric constant, in contrast to the system without the metamaterial plate. A hybrid metamaterial plate incorporating a tunable capacitor was employed in [19] to attain two distinct negative refractive index characteristics, specifically -1 and -3. The capacitor's settings were fine-tuned according to the receiving coil's position, enabling magnetic field concentration even in scenarios where the transmitting and receiving coils were misaligned. This adjustment resulted in an approximate 20% enhancement in transmission efficiency at a distance of 70 cm.

Misalignment of the magnetic couplers causes the coupling coefficient, to deviate from the nominal value, which affects the system's efficiency, output power, input phase angle, and input impedance. Thus, it is crucial to appropriately design the compensation network to maintain efficiency as high as possible and to reduce the sensitivity to the coupling variation [20]. Four basic compensation networks such as Series-Parallel (S-P), Parallel-Series (P-S), Series-Series (S-S), and Parallel-Parallel (P-P), are not appropriate for working under misalignment as they are highly susceptible to

misalignment. The series-series (SS) compensation topology is commonly employed as a general compensation network in EV wireless charging due to its resonance frequency independence from coupling and load condtions [21]. LCC compensation network has been introduced in the literature to improve misalignment tolerance, which not only keeps the resonant frequency independent of coupling coefficients and load conditions but also ensures high efficiency by operating in a zero-current switching state, maintaining stable performance even in cases of misalignment [22]. Authors in [23] proposed an approach for tuning compensation capacitance based on receiver misalignment by using switched capacitors.

Hybrid topologies incorporate the advantages of each topology and provide a system that is resilient to changes in the coupling coefficient [24]. A hybrid topology, merging aspects of both series-series (S-S) and inductor-capacitor-capacitor-parallel (LCC-P) configurations, has been proposed in [25] to improve tolerance to misalignment. Both the S-S and LCC-P topologies yield constant-current output. However, they exhibit opposite behaviors in response to misalignment; therefore, By integrating these two topologies, it becomes feasible to enhance the system's misalignment tolerance.

Generally, the control strategies to cope with the misalignment issue are divided into three categories: primary side control [26], secondary side control [27], and dual side control [28]. The goal of primary side control is to reduce the size and cost of the secondary side, and wireless communication is required to send data from the secondary side to the primary side for the controller. Wireless communication is prone to delay, inaccuracy which affects the operation of the controller. The primary side control can be realized by controlling the inverter or controlling an aditional dc-dc converter added to the primary side. Authors in [29] proposed a primary-side control method based on the phase-shift full-bridge inverter to achieve misalignment insensitivity, all without the need for additional components such as a DC-DC converter, composite compensation topology, or wireless communication modules. Most of these established primary-side control techniques commonly rely on wireless communication modules, including but not limited to Wi-Fi and Bluetooth. The advantage of the secondary side control is that it does not require communication, which is simple and robust. However, it requires an additional circuit at the secondary side installed under the chassis of the electric vehicle, which increases the weight and cost of electric vehicles. The secondary side control to address the misalignment can be realized by controlling the rectifier [30] or controlling the additional dc-dc converter at the secondary side [31]. Dual-side control is a control scheme that controls both sides at the same time, which increases the complexity.

The previous research for tackling the misalignment issue is limited to a small range of misalignment while in the real world, the misalignment occurs at a higher level which most of the methods in the literature become inefficient for high misalignment and which leads to providing an autonomous alignment in some few papers. A self-alignment mechanism is introduced in [32], which employs a transmitting coil with a tumbler structure, incorporating Nd-Fe-B magnets at the center of both transmitter and receiver coils to generate an aligning force. Nevertheless, this self-aligning method encounters several challenges, including difficulties in controlling and stabilizing attractive forces, the possibility of accidental attraction to foreign metallic objects, concerns related to demagnetization, and the introduction of additional eddy-current losses in the magnets. Authors in [33] used the magnetic force between transmitter and receiver to align the coil, which the transmitter coil is installed on a mechanical structure to ease self-alignment by providing a low friction path for movement. However, this system is limited to a small range of misalignment due to the limitation of the mechanical structure.

The previous research works are limited to the misalignment range, and at higher misalignment, these methods are inefficient. A self-aligning mechanism to be effective in aligning the transmitter coil to the receiver automatically in every misalignment condition, no matter how much misalignment occurs, is missing in the literature. The lack of such aligning mechanisms in the literature motivates our research group to propose a novel autonomous self-aligning system to address a wide range of misalignments in the stationary charging of electric vehicles. The autonomous self-aligning mechanism can be achieved by using a robot to align the transmitter coil to the receiver with the assistance of a magnetic field sensor to detect the magnetic field.

II. CIRCUIT TOPOLOGY

Figure 1 shows the circuit topology of the series compensated IPT system, in which a full-bridge inverter at the primary side fed the inductive coil through a compensation network. The compensation network is used to minimize reactive power to improve efficiency. The power can be transferred from the transmitter coil to the receiver coil through the magnetic field. A rectifier is used at the secondary side to convert ac to dc to supply the battery.

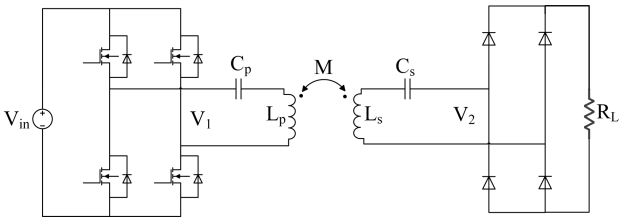

FIGURE 1. Circuit topology of the series compensated IPT system.

III. COIL STRUCTURE

Figure 2 shows the coil structure, which is a circular pad. Ferrite bars are used at the transmitter and receiver sides to improve the coupling coefficient. Aluminum plates are used on both sides for the shielding purpose.

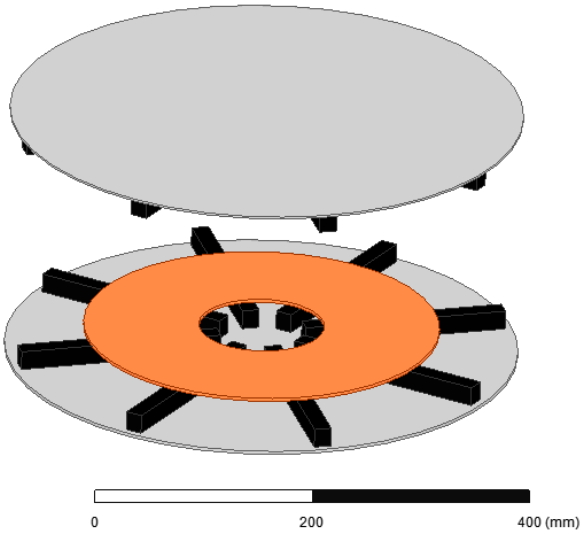

a) 3D view of the coil

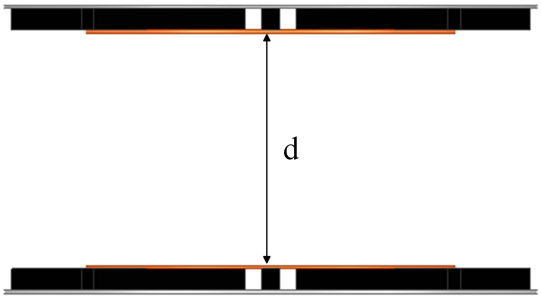

b) Front view of the coil

FIGURE 2. Structure of the coil.

The magnetic field in the center of the air gap at the well-aligned can be calculated as follows:

$$B = \frac{\mu_0 NIR^2}{2}\left(\frac{1}{\sqrt{R^2+\left(z-\frac{d^2}{8}\right)^2}}+\frac{1}{\sqrt{R^2+\left(z+\frac{d^2}{8}\right)^2}}\right) \tag{1}$$

where N is the number of turns, I is the current, R is the radius of the circular pad and d is the air gap. when there is misalignment in y direction as a length of d_y, the magnetic field at the center of the air gap is described as follows:

$$B = \frac{\mu_0 NIR^2}{2}\left(\frac{1}{\sqrt{R^2+\left(z-\frac{d^2}{8}\right)^2}} + \frac{1}{\sqrt{R^2+\left(z+\frac{\sqrt{(d^2/4+d_y^2)^2}}{4}\right)^2}}\right) \tag{2}$$

According to eq. 2, the magnetic field strength in the midpoint between transmitter and receiver is decreased by increasing misalignment (d_y). The mutual inductance between transmitter and receiver at misalignment can be calculated as follows:

$$M = \frac{\mu_0 \pi N^2 R^2}{2}\left(\frac{1}{\sqrt{R^2+\left(z-\frac{d^2}{8}\right)^2}} + \frac{1}{\sqrt{R^2+\left(z+\frac{\sqrt{(d^2/4+d_y^2)^2}}{4}\right)^2}}\right) \tag{3}$$

The primary current is derived as follows:

$$i_p = \frac{j\omega L_s + R_s + \frac{1}{j\omega C_s}V_{in}}{\left(R_p + \frac{1}{j\omega C_p} + j\omega L_p\right)\left(j\omega L_s + R_s + \frac{1}{j\omega C_s}\right) + \omega^2 M^2} \tag{4}$$

The output power and efficiency for a series-seies compensated IPT system is expressed as follows, eq. 5 and eq. 6, as shown at the bottom of the next page, where R_p and R_s are the resistance of the transmitter and receiver coil, respectively, and $R_{ac} = \frac{8}{\pi^2} R_L$. As misalignment between transmitter and receiver start to increase, the mutual inductance start to decrease, leading to drop in the efficiency. In other words, increasing misalignment gives rise to higher power losses in the IPT system. The total losses in the IPT system primarily comprise three parts: specifically, losses in the inverters, losses in the transmitter and receiver coils, and losses in the rectifiers. The losses of primary inverter mainly include conduction losses and switching losses of MOSFETs, which can be calculate as follows [34]:

$$\begin{aligned} P_{\text{con,loss}} &= \frac{r_{ds}}{\pi}\left(i_{p,\text{rms}}^2 + i_{a,\text{rms}}^2\right)(\pi+\theta+\sin(\theta)) \\ P_{\text{sw,loss}} &= 2V_{in}\left(i_{p,\text{rms}} + i_{a,\text{rms}}\right)\sqrt{2}\cos\left(\frac{\theta}{2}\right)f \\ &\quad \times \left(\frac{e_{\text{sw,on}} + e_{\text{sw,off}}}{V_R I_R}\right) \\ P_{\text{inv,loss}} &= P_{\text{con,loss}} + P_{\text{sw,loss}} \end{aligned} \tag{7}$$

where $e_{sw,on}$, $e_{sw,off}$, V_R, I_R, and r_{ds} are the turn-on, turn-off losses, drain-source voltage, drain-source current, and on-state resistance of primary of MOSFETs. According to eq. 4, a reduction in mutual inductance results in an increase in primary current, and in accordance with eq. 7, this causes a rise in power losses in the MOSFETs.

Inductive coupler losses comprise two main parts: copper losses (P_{cu}) and ferrite losses (P_{fe}). Copper losses consist of losses due to skin effects (P_{se}) and losses due to proximity

effects (P_{pe}), which are expressed as follows [35]:

$$\begin{aligned} P_{\text{se}} &= n_{\text{st}} R_{\text{dc}} F_R(f) \left(\frac{I_{\text{peak}}}{n_{\text{st}}}\right)^2 \\ P_{\text{pe}} &= n_{\text{st}} R_{\text{dc}} G_R(f) \left(H_e^2 + \frac{I_{\text{peak}}^2}{2\pi^2 d_a^2}\right) \\ P_{\text{cu}} &= P_{\text{se}} + P_{\text{pe}} \\ P_{\text{fe}} &= k_s f^{\alpha} B^{\beta} \end{aligned} \tag{8}$$

n_{st} represents the number of strands in the Litz wire, and R_{dc} denotes the DC resistance per unit length of a single strand of the Litz wire. I_{peak} stands for the transmitter's peak current, and $F_R(f)$ is a frequency-dependent factor accounting for the skin effect. d_a corresponds to the outer diameter of an individual strand of the Litz wire, $G_R(f)$ illustrates a frequency-dependent factor reflecting proximity effects, and H_e represents the external magnetic field that penetrates the windings. k_s, α, and β are Steinmetz parameters. The power loss in the rectifier can be calculated as follows:

$$P_{rec,loss} = \frac{2\sqrt{2}}{\pi} V_f i_s + r_D i_s^2 \tag{9}$$

Figure 3 demonstrates the magnetic field distribution in the well-aligned case and when the transmitter and receiver have 20cm misalignment.

As shown in Figure 3, when the transmitter coil is well-aligned with receiver coil, the magnetic field strength at the midpoint between the transmitter and receiver is 0.8 mT. While at the 20 cm misalignment, the magnetic field strength at the mid-point between the transmitter and receiver is half of the magnetic field value in a well-aligned case. This proves that the misalignment gives rise to a reduction in magnetic field strength at the air gap between the transmitter and receiver coils.

Figure 4 shows the energy distribution between transmitter and receiver coils at well-aligned and 20cm misalignment cases. Figure 4 verifies that the misalignment causes a decrease in energy transfer between the transmitter and receiver pads.

Figure 5 shows the coupling coefficient between the transmitter and receiver in different misalignments. As shown in Figure 5, the misalignment gives rise to a significant reduction in the coupling coefficient, in which at 25cm misalignment, the coupling coefficient reaches zero.

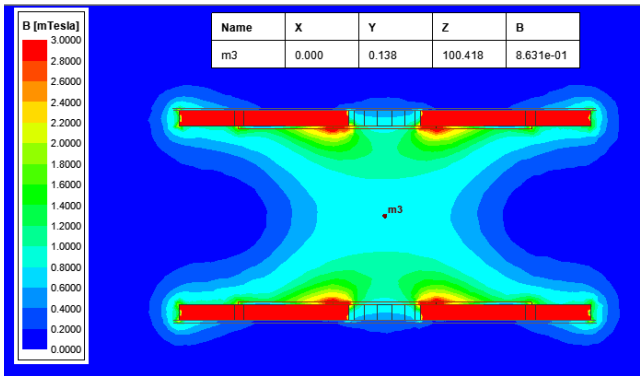

a) Magnetic field distribution at well-aligned

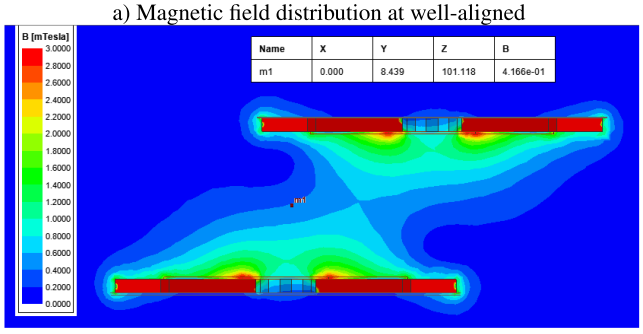

b) Magnetic field distribution at 20cm misalignment

FIGURE 3. Magnetic field distribution.

IV. PROPOSED AUTONOMOUS ALIGNMENT SYSTEM

To improve the misalignment performance, an autonomous self-alignment system is proposed, in which the transmitter pad is mounted on a robot to follow receiver pad. A magnetic field sensor is installed on the transmitter pad, which follows the highest magnetic field value. The highest magnetic field is in the well-aligned case, which the transmitter and receiver are well-aligned. In this case, by having misalignment, the transmitter pad moves to remove misalignment and create alignment. In other words, the transmitter follows the receiver to remove misalignment. Figure 6 shows the structure of the proposed system. As shown in Figure 6, the transmitter coil is mounted on a robot to move the transmitter. A magnetic field sensor is installed on the transmitter pad to measure the magnetic field. The measured magnetic field is compared with the highest magnetic field value, and the error sends to the controller. The controller sends a command to the robot to move the transmitter pad to reduce the error to make alignment with the receiver pad.

$$P = R_{ac} \left[\frac{\omega M V_{in}}{\left(R_p + j\omega L_p + \frac{1}{j\omega C_p}\right) \cdot \left(R_{ac} + R_s + j\omega L_s + \frac{1}{j\omega C_s}\right) + (\omega M)^2} \right]^2 \tag{5}$$

$$\eta = \frac{R_{ac}}{R_{ac} + R_s + R_p \left(\frac{R_{ac} + R_s + j\omega L_s + \frac{1}{j\omega C_s}}{\omega^2 M^2}\right)} \tag{6}$$

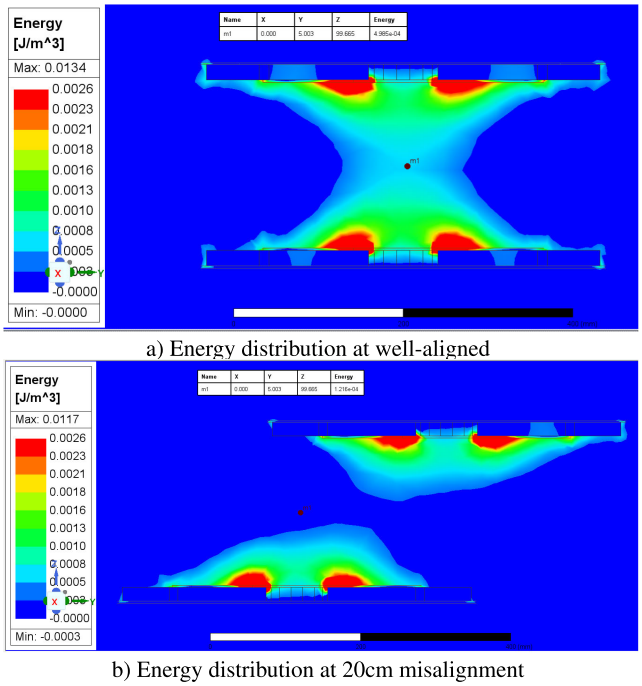

FIGURE 4. Energy distribution between transmitter and receiver pads.

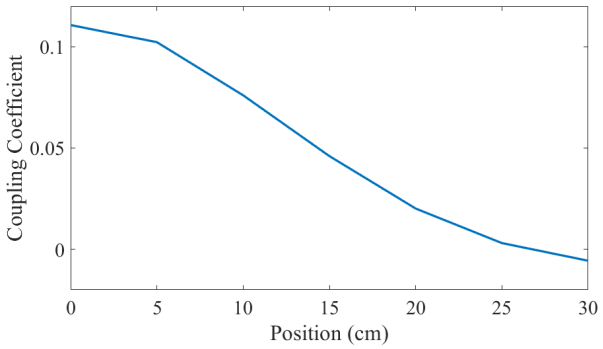

FIGURE 5. Coupling coefficient between transmitter and receiver at different misalignment.

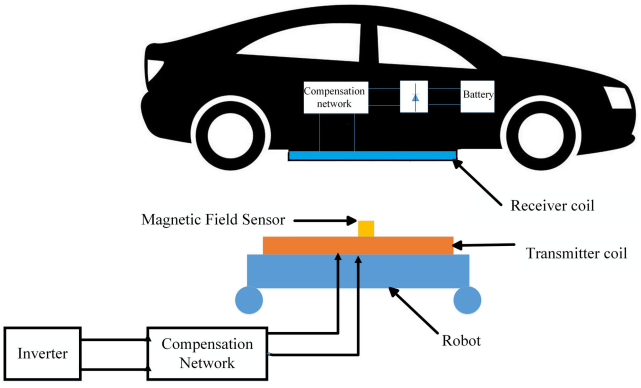

FIGURE 6. The structure of the proposed autonomous alignment system.

Fig. 7 shows the interaction between the magnetic field sensor and the magnetic flux generated by the receiver pad at

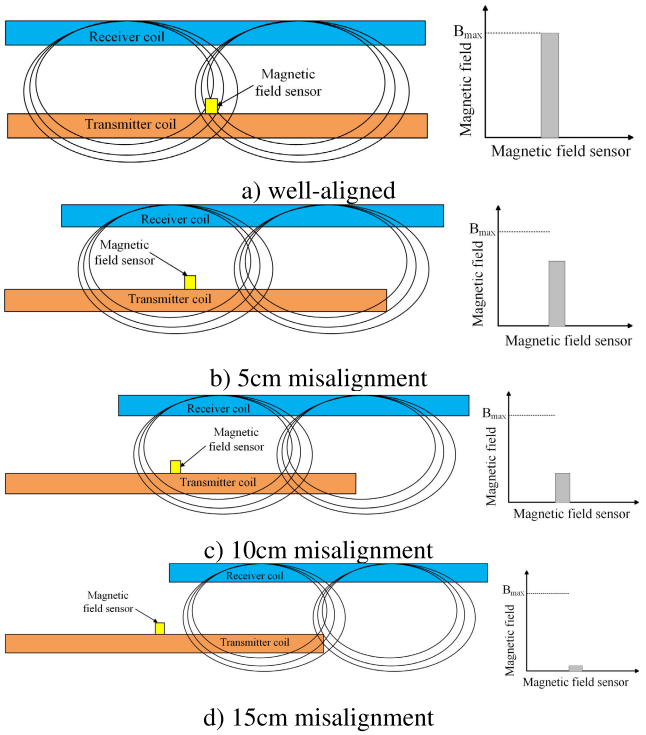

FIGURE 7. Interaction between the magnetic field sensor and the magnetic flux generated by the receiver coil.

different misalignment conditions. It is evident that the sensor measures the highest magnetic field at well-aligned, and by increasing the misalignment, the magnetic field is decreasing.

A. DESIGN PROCESS OF THE ROBOT'S STRUCTURE

The robot should be designed properly, so that can tolerate the weight of the transmitter coil without affecting the speed and movement of the robot. In this section, the design process of the robot is discussed in detail. The chassis of robot is made of a Galvanized Steel Frame that goes around in an octagonal shape. This frame is strong enough to support the transmitter coil and is a solid foundation for all the other parts that would be implemented. Figure 8 (a) shows the structure of the Galvanized steel frame.

The frame then is supported additionally by another bar in the middle that contributes to better stability and strength. This steel bar also holds the motors and the motors are off-brand 12V motors with high torque. Because of the torque, it can handle a large sum of weight. With the 4-inch size of the wheels on the motors, the total platform can haul a little over 35 pounds. The downside of this type of motor is that it is not very fast, but it is still able to push the required amount of weight. Figure 8 (b) shows the steel bars holding the motors.

This frame supports a PVC platform that holds the transmitter coil and the magnetic field sensor. Underneath this platform, another PVC platform is created to house other components, such as battery packs and microcontrollers. The frame is supported by two wheels powered by 12V motors

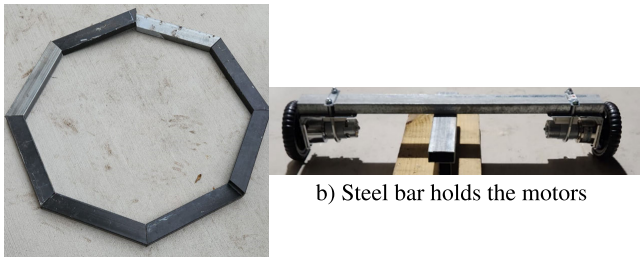

a) Galvanized steel frame

b) Steel bar holds the motors

FIGURE 8. Robot components.

and 4 Caster Wheels. The caster wheels give the flexibility to move and allow for good stability while providing a firm foundation.

All these components came together to get the current version of the alignment system's chassis. This chassis is very strong and durable. It has the space and strength to hold the transmitter coil and all other components. The overall chassis weighs around 30 pounds with the transmitter coil. Figure 9 shows the complete chassis for holding the transmitter coil.

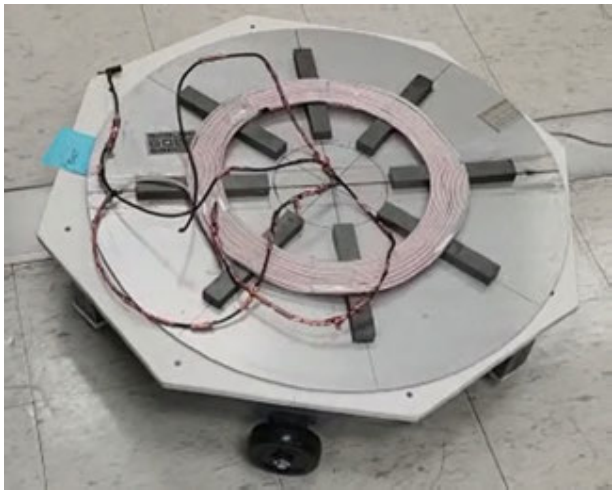

FIGURE 9. Completed chassis for holding transmitter coil.

B. THE CONTROL MECHANISM OF THE SELF-ALIGNING SYSTEM

Figure 10 shows the block diagram of the proposed autonomous self-aligning mechanism. The entire system takes in two inputs and has one output. An existing magnetic field will be taken as an input to the magnetic field strength detection unit. The transmitter coil within the detection unit will use its own power supply to contribute to the strength of the existing magnetic field. The microcontroller receives magnetic field strength values from the hall effects sensor, which it then uses to perform calculations and logic on those values and outputs motor instructions. Since the motors cannot understand these instructions, the motor shield serves as the interface that translates these instructions for the motors to adjust the chassis position accordingly.

This section focuses on a highly specialized algorithm that is specifically designed to control the EV wireless charging alignment system. This algorithm is critical in aligning the transmitter coil to the receiver coil to maximize their power transfer. This algorithm's unique and complex nature demands exceptional attention and understanding to ensure the effective functioning of the charging device. This section will delve deeply into the inner workings of this algorithm and explore its intricacies and nuances to gain a comprehensive understanding of its capabilities and limitations. It will explain the algorithm in detail, including its functionality, applications, and notable characteristics. By providing an in-depth analysis of this algorithm, this section aims to provide a comprehensive understanding of its workings, potential, and limitations and to highlight its importance in the field of electric vehicle wireless charging.

This section also explains the algorithm that is fully developed and tested. The concept for this algorithm is designed to be as straightforward as possible to follow a test-driven development (TDD) and Agile approach, even though no test harnesses were used in conglomeration with the Arduino integrated development environment (IDE). This simplicity has several advantages with respect to the goal and expectations of this product as well as the current development stage. The following are some general goals and expectations that drove the decision to take a simplistic approach and were taken into consideration when developing the algorithms.

For realizing an autonomous self-aligning mechanism, a forward single-axis algorithm is used and tested in the laboratory setting. This algorithm, when powered on, tells the motors to move forward. The alignment system will then move forward until a hardcoded setpoint value is received from the sensor. When the microcontroller gets the setpoint value from the sensor, it will tell the motors to stop. This only goes in one direction, which in this paper is implemented to move in y direction.

Figure 12 shows the implemented proposed algorithm in the real world. As shown in Figure 12, onto the chassis, two 12V motors were fitted onto the sides to propel the chassis in the desired direction. These motors were connected to the 3A L298N motor drive shield. The motor drive shield is robust enough to support the battery pack that powers the motors. The motor shield also allows for better controllability of the individual motors by providing individual settings for the direction and speed of each motor. This motor drive shield takes power from the battery pack and powers the motor.

The motor drive shield gets instructions from the Arduino Mega 2560 Microcontroller to move the motors according to the implemented algorithm. The Arduino Mega is more than capable of executing the instructions that is given to it. Since it is a larger controller, it has the space to accommodate for additional features that could be implemented in the future such as more sensors.

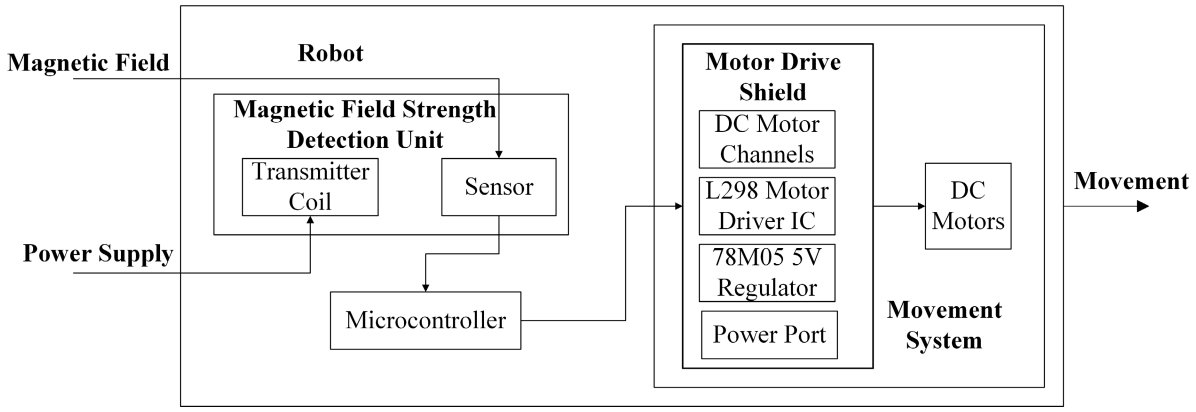

FIGURE 10. Block diagram of the proposed autonomous self-aligning system.

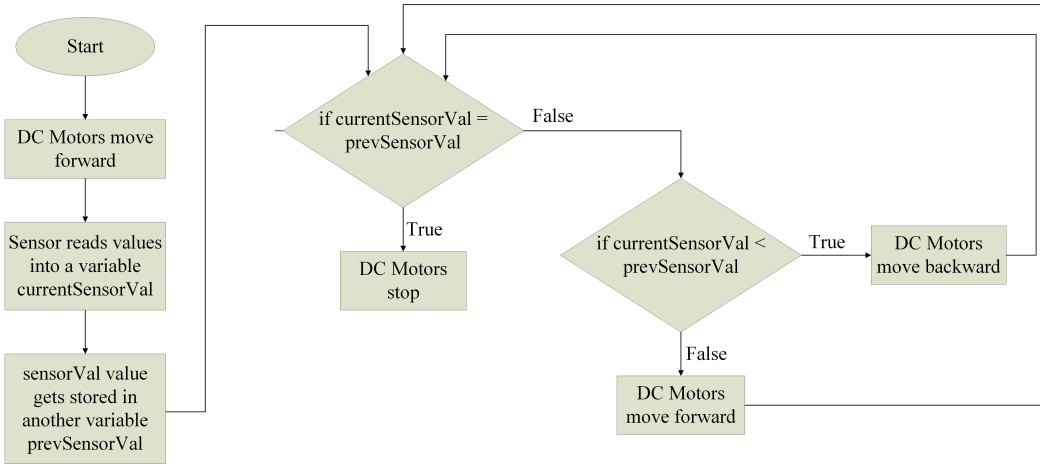

FIGURE 11. Flowchart of the forward single-axis algorithm.

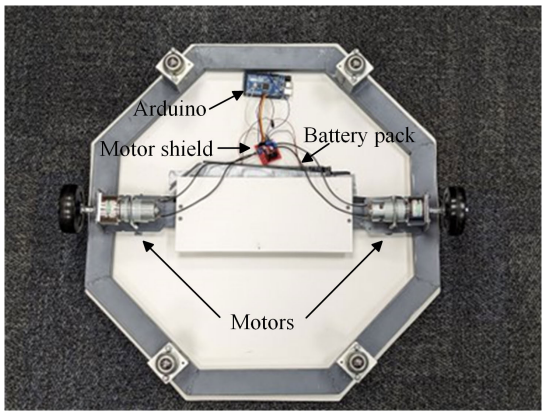

FIGURE 12. Implemented proposed algorithm in the real world.

The Arduino Mega 2560 Microcontroller processes logic based on the sensor values that are obtained through the hall effect sensor that is attached to the top of the alignment system. The Hall effect sensor is able to read the values from the magnetic field that the coils produce and accurately gives those values to the Arduino Mega 2560 to use.

V. EXPERIMENTAL RESULTS

After designing the coupler, the circuit parameters are tuned for realizing resonance at the frequency of 35 kHz. TABLE 1 shows the coupler's dimensions and circuit specifications.

TABLE 1. Coupler's dimension and circuit specification.

Parameter	Value	Parameter	Value
V_{in},V_{out}	25 V	f	35 kHz
Coil's internal dia	117 mm	Width of the coil	107 mm
Ferrite bar length	192 mm	Ferrite bar width	18 mm
Shielding plate dia	750 mm	Number of turns	15
L_p, L_s	172 μH	C_s, C_p	120 nF
Air gap (d)	200 mm	Load resistor (R_L)	5 Ω

Using the parameters in the TABLE 1, a prototype of the system is constructed which is shown in Figure 13.

The transmitter and receiver coil are composed of AWG 36 Litz wire to minimize skin effect losses. For the

FIGURE 13. Experimental prototype of the system.

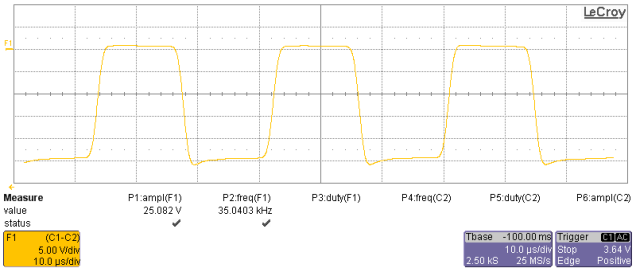

FIGURE 14. Output voltage of inductive power transfer.

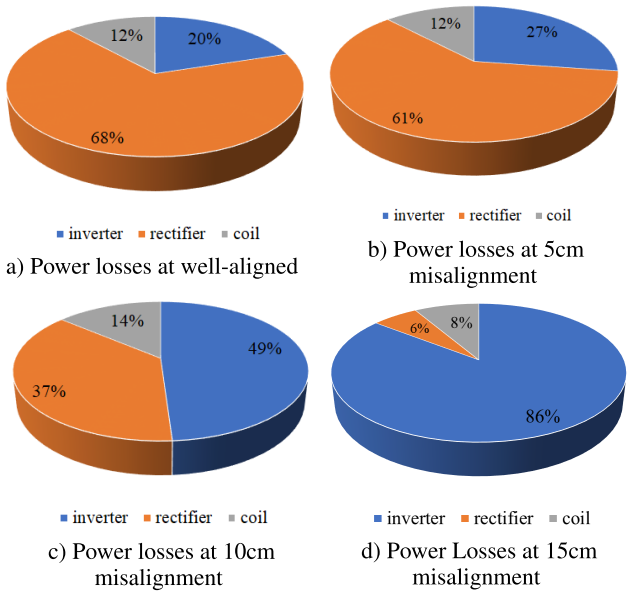

FIGURE 15. Power losses percentage of three parts contributing in power losses generation.

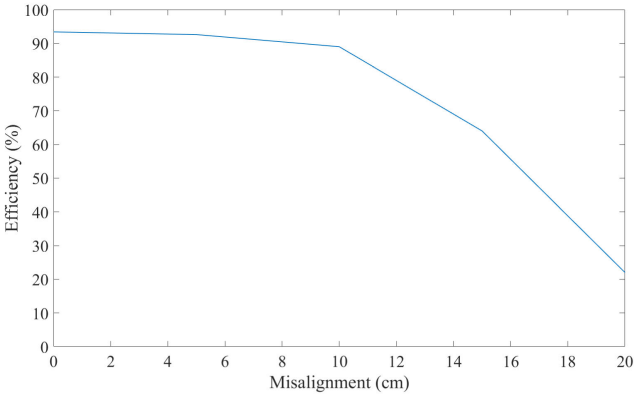

FIGURE 16. Efficiency of the IPT system without using the proposed self-alignment mechanism.

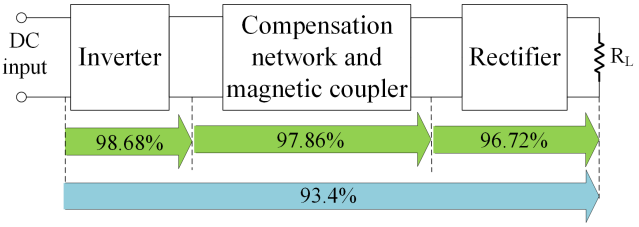

FIGURE 17. Power losses at different section of IPT system when deploying the proposed self-aligning mechanism.

implementation of the input inverter, silicon-carbide (SiC) MOSFETs C2M0025120D are utilized to minimize conduction losses. Texas Instruments TMS320F28379D digital microcontroller is used for the generation of the MOSFETs PWM signals. The digital microcontroller has the advantage of being convenient in adjusting the frequency and dead time for the full-bridge inverter. In this paper, the dead time is selected to be 100ns. Figure 14 shows the output voltage of the inductive power transfer.

Figure 15 displays the power loss percentages associated with three contributing parts in power losses generation. It's clear that increasing misalignment leads to a greater dominance of inverter losses in overall power loss. This shift towards increased inverter losses is because inverter losses are directly proportional to square of the primary current, as indicated in eq. 7. Misalignment causes a rise in primary current, as demonstrated in eq. 4, thereby causing higher losses in the inverter.

Figure 16 shows the efficiency of the IPT system at different misalignment conditions without using the proposed self-alignment mechanism, in which at well-aligned achieved the highest efficiency (93.4%), and by increasing the misalignment, the efficiency dropped. While using the proposed self-alignment mechanism maintain the efficiency at 93.4%. It is important to emphasize that the robot is powered by a combined 24V battery pack (two 12V batteries), and the supply of power to the robot itself does not introduce any significant power losses.

The required voltage and current for powering each motor are 12V and 3A, respectively. As the robot incorporates two motors, the power consumption for feeding the robot can be calculated as follows:

$$P_{robot} = 2 * V.I = 2 * 12 * 3 = 72W \tag{10}$$

This power is supplied from an external battery pack installed beneath the robot chassis. This implies that the power does not come from the inductive charging system, and as such, it does not affect the efficiency of the IPT system. It should

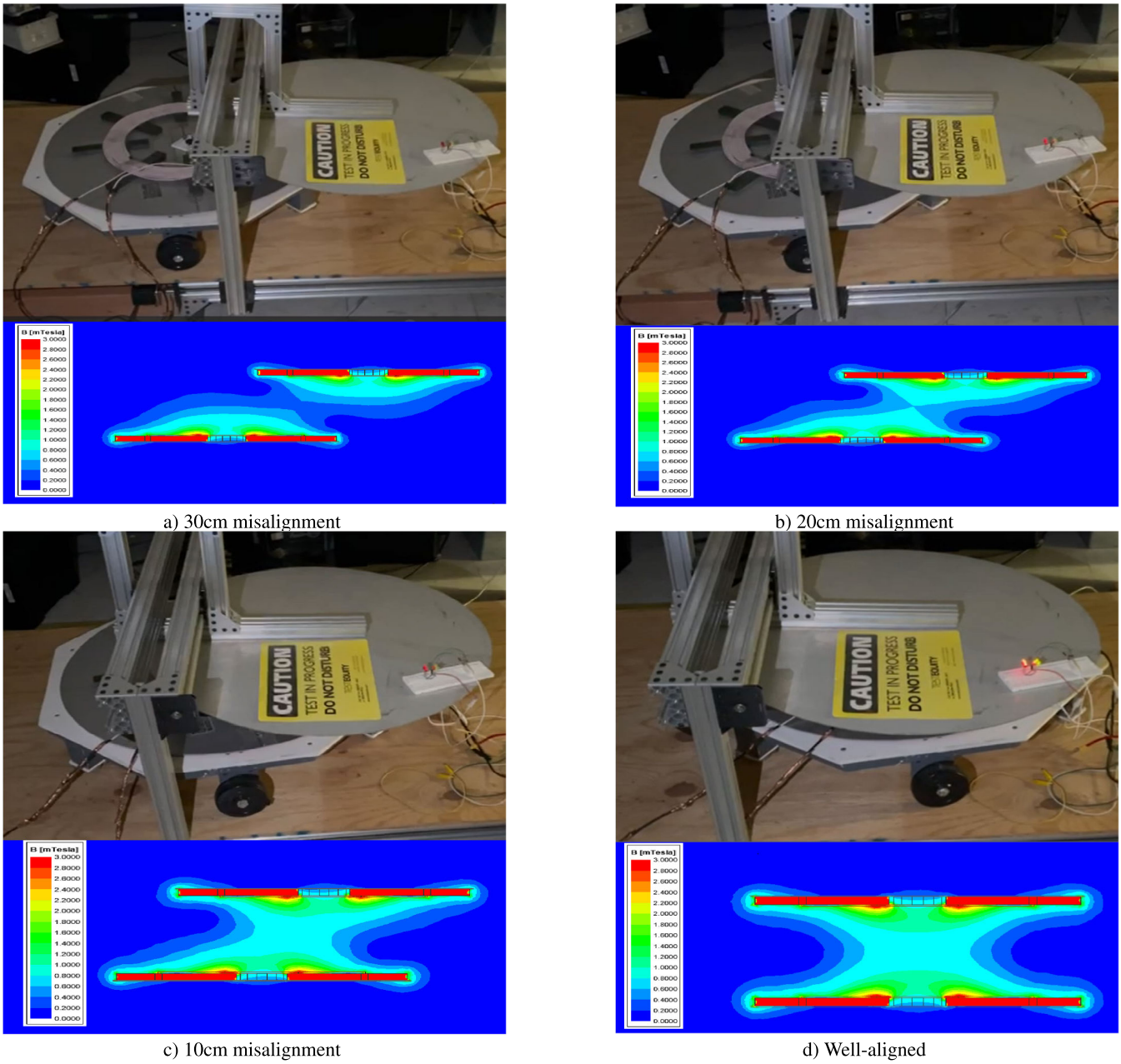

a) 30cm misalignment

b) 20cm misalignment

c) 10cm misalignment

d) Well-aligned

FIGURE 18. **Experimental results.**

be noted that the robot only consumes power for a short period during misalignment. Once full alignment is reached, the robot stops working and remains unpowered, especially during the charging process.

Figure 17 displays the losses in each section of the IPT system with the implementation of the proposed alignment mechanism. The robot does not draw power from the IPT system, as it does not have any electrical or magnetic connection with the IPT system, thereby not affecting the efficiency of the system. Moreover, when full alignment is achieved, the robot stops working and is not powered during the operation of the IPT system.

To test the effectiveness of the proposed autonomous self-aligning mechanism, the receiver is placed with 30 cm misalignment with respect to the transmitter coil mounted on the robot. The magnetic field sensor at the center of the transmitter's coil reads the magnetic field value, and by using the proposed algorithm, the robot moves forward to find the magnetic field value at the well-aligned. When the transmitter's coil mounted on the robot reach the alignment point, the robot is stopped. The alignment is created automatically and without human interference. Figure 18 shows the experimental results of the autonomous self-aligning mechanism as the transmitter's coil on the robot

automatically follows the receiver to make the alignment. A video of the robot's movement toward the receiver is created, but it is not possible to provide a video in the PDF. Due to this reason, a snapshot of 4 different misalignment cases is provided with the respective magnetic field distribution in Figure 18. Five LEDs are connected in series at the output side of the inductive power transfer to show whether the power is transferred or not in different misalignment cases. It is worth mentioning that these five LEDs are connected in series; therefore, 25V is required to turn the LEDs on. As shown in Figure 18(a), the receiver is placed with a 30 cm misalignment, in which the LEDs are off, indicating that no power is transferring. The robot starts traveling toward the receiver to find full alignment by comparing the magnetic field value sensed by the magnetic field sensor at the time with the highest value of the magnetic field. The snapshot of its movement at 20 cm misalignment is provided in Figure 18(b), where a relative alignment is created, and the magnetic field sensor senses a weak magnetic field, which turns a few LEDs on with a dim light. The robot moves further so that the sensor can read the high magnetic field close to the value in the well-aligned case, and its snapshot at 10cm misalignment is shown in Figure 18(c). Since a partial alignment occurs at 10cm misalignment, the sensor can sense the magnetic field in the partial alignment, so some of the LEDs are turned on. The robot moves further to find well-alignment, and as the full alignment happens as the sensor senses the highest magnetic field strength, the robot stops. At this point, which is shown in Figure 18(d), all the LEDs turn on, meaning that full power is transferred.

VI. CONCLUSION AND FUTURE WORKS

An autonomous self-aligning mechanism for addressing misalignment issue in the stationary wireless charging of electric vehicles is proposed. The proposed mechanism uses a robot to move the transmitter to follow the receiver pad based on measuring the magnetic field. The design process of the robot by considering the transmitter's coil weight and the required torque for the dc motors to move the transmitter's coil is discussed in detail. Three algorithms are proposed for self-aligning the transmitter coil to the receiver coil, and the forward self-aligned algorithm is implemented in the laboratory. The experimental results validate the effectiveness of the proposed autonomous self-aligning mechanism in making alignment between the transmitter's coil and receiver coil. The future work lines into implementing a double single-axis algorithm in the laboratory, which addresses the horizontal and vertical misalignment problem.

ACKNOWLEDGMENT

The authors acknowledge the support provided by the senior design team (Christopher Prasad, Maximiliano Mauna, Andy Alvarez, Rodolfo Ramos, and Ivan Mendoza) in theory and experimental work.

REFERENCES

[1] Y. Zhang, W. Pan, H. Wang, Z. Shen, Y. Wu, J. Dong, and X. Mao, "Misalignment-tolerant dual-transmitter electric vehicle wireless charging system with reconfigurable topologies," *IEEE Trans. Power Electron.*, vol. 37, no. 8, pp. 8816–8819, Aug. 2022.

[2] A. Sagar, A. Kashyap, M. A. Nasab, S. Padmanaban, M. Bertoluzzo, A. Kumar, and F. Blaabjerg, "A comprehensive review of the recent development of wireless power transfer technologies for electric vehicle charging systems," *IEEE Access*, vol. 11, pp. 83703–83751, 2023.

[3] M. Behnamfar, H. Javadi, and E. Afjei, "A dynamic CPT system LC compensated with a six-plate capacitive coupler for wireless charging of electric vehicle in motion," in *Proc. 28th Iranian Conf. Electr. Eng. (ICEE)*, Iran, Aug. 2020, pp. 1–6.

[4] J. Rahulkumar, R. Narayanamoorthi, P. Vishnuram, C. Balaji, T. Gono, T. Dockal, R. Gono, and P. Krejci, "A review on resonant inductive coupling pad design for wireless electric vehicle charging application," *Energy Rep.*, vol. 10, pp. 2047–2079, Nov. 2023.

[5] A. Mahesh, B. Chokkalingam, and L. Mihet-Popa, "Inductive wireless power transfer charging for electric vehicles—A review," *IEEE Access*, vol. 9, pp. 137667–137713, 2021.

[6] Z. Huang, S.-C. Wong, and C. K. Tse, "Control design for optimizing efficiency in inductive power transfer systems," *IEEE Trans. Power Electron.*, vol. 33, no. 5, pp. 4523–4534, May 2018.

[7] V.-B. Vu, A. Ramezani, A. Triviño, J. M. González-González, N. B. Kadandani, M. Dahidah, V. Pickert, M. Narimani, and J. Aguado, "Operation of inductive charging systems under misalignment conditions: A review for electric vehicles," *IEEE Trans. Transport. Electrific.*, vol. 9, no. 1, pp. 1857–1887, Mar. 2023.

[8] K. Song, G. Yang, Y. Guo, Y. Lan, S. Dong, J. Jiang, and C. Zhu, "Design of DD coil with high misalignment tolerance and low EMF emissions for wireless electric vehicle charging systems," *IEEE Trans. Power Electron.*, vol. 35, no. 9, pp. 9034–9045, Sep. 2020.

[9] J. Domajnko and N. Prosen, "A wireless power transfer system using a double DD quadrature coil structure," *Electronics*, vol. 12, no. 4, p. 890, Feb. 2023.

[10] N. Rasekh, J. Kavianpour, and M. Mirsalim, "A novel integration method for a bipolar receiver pad using LCC compensation topology for wireless power transfer," *IEEE Trans. Veh. Technol.*, vol. 67, no. 8, pp. 7419–7428, Aug. 2018.

[11] B. M. Mosammam and M. Mirsalim, "New integrated tripolar pad using double-sided LCC compensation for wireless power transfer," *IEEE Trans. Veh. Technol.*, vol. 69, no. 12, pp. 15633–15643, Dec. 2020.

[12] L. Zhao, D. J. Thrimawithana, U. K. Madawala, A. P. Hu, and C. C. Mi, "A misalignment-tolerant series-hybrid wireless EV charging system with integrated magnetics," *IEEE Trans. Power Electron.*, vol. 34, no. 2, pp. 1276–1285, Feb. 2019.

[13] P. Zhang, M. Saeedifard, O. C. Onar, Q. Yang, and C. Cai, "A field enhancement integration design featuring misalignment tolerance for wireless EV charging using LCL topology," *IEEE Trans. Power Electron.*, vol. 36, no. 4, pp. 3852–3867, Apr. 2021.

[14] K. Shi, T. Feng, J. Jiang, P. Wang, Z. Meng, and C. Tang, "A highly magnetic integrated method of LCC-compensated IPT system with excellent misalignment tolerance," *IEEE Trans. Power Electron.*, vol. 38, no. 12, pp. 16256–16268, Dec. 2023.

[15] M. Behnamfar, H. Jafari, and A. Sarwat, "Development of a mixed inductive and capacitive wireless power transfer to improve misalignment performance for charging electric vehicles," in *Proc. IEEE Transp. Electrific. Conf. Expo. (ITEC)*, Jun. 2022, pp. 600–605.

[16] M. S. Yusri, M. H. Misran, N. Yusop, M. A. M. Said, M. A. Othman, and S. Suhaimi, "Transfer efficiency enhancement on wireless power transfer using metamaterial," in *Proc. Int. Conf. Inf. Technol. (ICIT)*, Aug. 2023, pp. 724–729.

[17] C. Rong, L. Yan, L. Li, Y. Li, and M. Liu, "A review of metamaterials in wireless power transfer," *Materials*, vol. 16, no. 17, p. 6008, Aug. 2023.

[18] T. Shaw and D. Mitra, "Wireless power transfer system based on magnetic dipole coupling with high permittivity metamaterials," *IEEE Antennas Wireless Propag. Lett.*, vol. 18, pp. 1823–1827, 2019.

[19] W. Lee and Y.-K. Yoon, "Tunable metamaterial slab for efficiency improvement in misaligned wireless power transfer," *IEEE Microw. Wireless Compon. Lett.*, vol. 30, no. 9, pp. 912–915, Sep. 2020.

[20] A. Ramezani and M. Narimani, "Optimized electric vehicle wireless chargers with reduced output voltage sensitivity to misalignment," *IEEE J. Emerg. Sel. Topics Power Electron.*, vol. 8, no. 4, pp. 3569–3581, Dec. 2020.
[21] Z. Yuan, M. Saeedifard, C. Cai, Q. Yang, P. Zhang, and H. Lin, "A misalignment tolerant design for a dual-coupled LCC-S-compensated WPT system with load-independent CC output," *IEEE Trans. Power Electron.*, vol. 37, no. 6, pp. 7480–7492, Jun. 2022.
[22] J. C. Quirós, E. V. Guerrero, J. K. Sangeno, and A. Triviño, "Magnetic integration of circular pads and LCC-LCC for EV wireless charging tolerant to misalignment," *IEEE Access*, vol. 11, pp. 98558–98565, 2023.
[23] K. A. Cota, P. A. Gray, M. Pathmanathan, and P. W. Lehn, "An approach for selecting compensation capacitances in resonance-based EV wireless power transfer systems with switched capacitors," *IEEE Trans. Transport. Electrific.*, vol. 5, no. 4, pp. 1004–1014, Dec. 2019.
[24] W. Zhao, X. Qu, J. Lian, and C. K. Tse, "A family of hybrid IPT couplers with high tolerance to pad misalignment," *IEEE Trans. Power Electron.*, vol. 37, no. 3, pp. 3617–3625, Mar. 2022.
[25] Y. Zhang, Z. Huang, H. Wang, C. Liu, and X. Mao, "Achieving misalignment tolerance with hybrid topologies in electric vehicle wireless charging systems," *Energy Rep.*, vol. 9, pp. 259–265, Sep. 2023.
[26] F. Farajizadeh, D. M. Vilathgamuwa, D. Jovanovic, P. Jayathurathnage, G. Ledwich, and U. Madawala, "Expandable N-legged converter to drive closely spaced multitransmitter wireless power transfer systems for dynamic charging," *IEEE Trans. Power Electron.*, vol. 35, no. 4, pp. 3794–3806, Apr. 2020.
[27] J. Liu, Z. Liu, and H. Su, "Passivity-based PI control for receiver side of dynamic wireless charging system in electric vehicles," *IEEE Trans. Ind. Electron.*, vol. 69, no. 1, pp. 783–794, Jan. 2022.
[28] M. Kim, D.-M. Joo, and B. K. Lee, "Design and control of inductive power transfer system for electric vehicles considering wide variation of output voltage and coupling coefficient," *IEEE Trans. Power Electron.*, vol. 34, no. 2, pp. 1197–1208, Feb. 2019.
[29] Z. Li, H. Liu, Y. Tian, and Y. Liu, "Constant current/voltage charging for primary-side controlled wireless charging system without using dual-side communication," *IEEE Trans. Power Electron.*, vol. 36, no. 12, pp. 13562–13577, Dec. 2021.
[30] S. Ann, J. Byun, W.-J. Son, J. H. Lee, and B. Kuk Lee, "Impedance tuning control and synchronization technique for semi-bridgeless active rectifier of IPT system in EV applications," in *Proc. IEEE Appl. Power Electron. Conf. Expo. (APEC)*, Mar. 2020, pp. 1622–1626.
[31] Y. Tian, Z. Li, H. Liu, Y. Liu, and M. Ban, "High-performance wireless charging system using interleaved buck converter and integrated solenoid magnetic coupler," *IEEE Trans. Transport. Electrific.*, vol. 9, no. 3, pp. 3821–3835, Sep. 2023.
[32] S. Ding, W. Niu, and W. Gu, "Lateral misalignment tolerant wireless power transfer with a tumbler mechanism," *IEEE Access*, vol. 7, pp. 125091–125100, 2019.
[33] A. Namadmalan, R. Tavakoli, S. M. Goetz, and Z. Pantic, "Self-aligning capability of IPT pads for high-power wireless EV charging stations," *IEEE Trans. Ind. Appl.*, vol. 58, no. 5, pp. 5593–5601, Sep. 2022.
[34] X. Wang, J. Xu, M. Mao, and H. Ma, "An LCL-based SS compensated WPT converter with wide ZVS range and integrated coil structure," *IEEE Trans. Ind. Electron.*, vol. 68, no. 6, pp. 4882–4893, Jun. 2021.
[35] V.-B. Vu, M. Dahidah, and V. Pickert, "Efficiency-cost parametric-analysis of a three-phase wireless dynamic charging system for electric vehicles," *IEEE J. Emerg. Sel. Topics Ind. Electron.*, vol. 3, no. 3, pp. 482–491, Jul. 2022.

MILAD BEHNAMFAR (Graduate Student Member, IEEE) received the B.S. degree in electrical engineering from the University of Kurdistan, in 2016, and the M.S. degree in power electronics and electric machines from Shahid Beheshti University, in 2018. He is currently pursuing the Ph.D. degree with Florida International University. He is a Research Assistant with the Energy, Power, Sustainability, and Intelligence (EPSi) Laboratory. His main research interests include wireless power transfer for the application of electric vehicle charging, high-frequency converters, power electronics, and control theories. He is a regular reviewer of the IEEE journals and conferences.

MOHD TARIQ (Senior Member, IEEE) received the bachelor's degree in electrical engineering from AMU, Aligarh, the master's degree in machine drives and power electronics from IIT Kharagpur, and the Ph.D. degree in electrical engineering from Nanyang Technological University (NTU), Singapore. He is currently a Faculty Member/Postdoctoral Associate with Florida International University, working on high-penetration renewable systems, grid resiliency, large-scale data analysis, artificial intelligence, electric vehicles, and cybersecurity. He is also an Assistant Professor (on leave) with AMU, where he directed various international and national sponsored research projects worth approximately 18 million INR and led a team of multiple researchers in the domain of power converters, energy storage devices, and their optimal control for electrified transportation and renewable energy application. He has authored more than 225 research papers in international journals/conferences, including many articles in IEEE TRANSACTIONS/journals. He is also an inventor of more than 25 patents granted/published by the patent offices of USA, Australia, U.K., Europe, India, and China. He is an Associate Editor of IEEE ACCESS, an Editorial Board Member of *Scientific Reports* and *Nature*, and a guest editor of various other journals.

ARIF I. SARWAT (Senior Member, IEEE) is currently an Eminent Scholar Chaired Professor with the Department of Electrical and Computer Engineering, and the Director of the FPL-FIU Solar Research Facility, Florida International University, Miami, FL, USA. He is also the Principal Investigator of the State-of-the-Art Grid-Connected 3MW/9 MWH AI-Based Renewable Microgrid Project funded by FPL. He has authored or coauthored more than 200 peer-reviewed articles and multiple patents. His research interests include smart grids, electric vehicles, high penetration renewable systems, storage, and battery management systems, grid resiliency, large-scale data analysis, artificial intelligence, advanced metering infrastructure, smart city infrastructure, and cybersecurity. He has multiple funded projects, funded by the National Science Foundation, industry, and the Department of Energy. He is the author or coauthor of a publication that won the Best Paper Award at the Resilience Week, in 2017, and a technical article that won both the Best Paper Award, in 2016, and the Most Cited Paper Award, in 2018, from *Journal of Modern Power Systems and Clean Energy* (Springer). He was a recipient of the Faculty Award for Excellence in Research, Creative Activities, in 2016; the College of Engineering and Computing Worlds Ahead Performance, in 2016; and the FIU TOP Scholar Award, in 2015 and 2019. Since 2012, he has been the Chair of the IEEE Miami Section VT and Communication. He is an Associate Editor of the IEEE TRANSACTIONS OF INDUSTRY APPLICATIONS and *ACM Computing Surveys*.